



# Fatigue damage tolerance of two tapered composite patch configurations



Chao Wu<sup>a,b</sup>, Andrew J. Gunnion<sup>b,c</sup>, Bernard Chen<sup>a</sup>, Wenyi Yan<sup>a,\*</sup>

<sup>a</sup> Department of Mechanical and Aerospace Engineering, Monash University, Clayton, Vic. 3168, Australia

<sup>b</sup> Cooperative Research Centre for Advanced Composite Structures Ltd., 1/320 Lorimer Street, Port Melbourne, Vic. 3207, Australia

<sup>c</sup> Advanced Composite Structures Australia, 1/320 Lorimer Street, Port Melbourne, Vic. 3207, Australia

## ARTICLE INFO

### Article history:

Available online 3 September 2015

### Keywords:

Damage tolerance  
Fatigue  
Skin doubler repair  
Stepped doubler repair  
Ply-drop doubler repair

## ABSTRACT

To avoid high peel stresses around the perimeter of a bonded composite patch repair, the patch thickness often tapers to a fine edge. This paper investigates and compares the damage tolerance of two different configurations of taper design under fatigue loading with different size of initial bondline flaws. The bondline damage at the tip of the doubler repair was simulated by an initial flaw which was created through a Teflon tape. A constant amplitude fatigue loading was applied to all specimens. The crack propagation against the number of cycles was recorded and the fatigue life when the crack reached 100 mm from the doubler tip was reported. Microscope investigations were conducted and provided micro scale evidence on the effects of initial flaw size on the crack initiation pattern of the two doubler design configurations. Finally, the damage tolerance of the two configurations were compared and conclusions were drawn with implications for the design of composite patch repairs. It was found that ply-drop doubler joints showed better damage tolerance than stepped doubler joints under fatigue loading. The experimental results suggested a threshold size of 5 mm for the doubler tip flaw, if any inspection technology should be adopted for damage detection.

© 2015 Elsevier Ltd. All rights reserved.

## 1. Introduction

Fibre reinforced polymer (FRP) composites have been adopted as construction materials for automotive, aerospace, civil and marine structures [1–5]. Suitable methods are required when repairing damaged composite parts [6–10] to restore their designed capacities. Two methods are currently widely adopted in composite structures, namely mechanical fastening and adhesive bonding. It has been widely reported that adhesive bonding has benefits such as lighter weight, better load transferring mechanism through larger bonded area and better fatigue performance [1,11–16]. On the other hand, mechanical fastening methods using bolts or rivets were always criticised due to stress concentration resulting from fibre cutting at bolt holes, and increasing the self-weight of structure [1,14,17]. The weight saving is especially more important in modern airplane structures where FRP composites become more extensively used (e.g. Boeing 787 with about 50% FRP by weight [18]), which makes the adhesive bonding methods more desirable [14].

There has been an increase in the demand of replacing mechanically fastened metallic patches with bonded composite patch

repair to increase the service life in aircraft operations [19,20]. However, as there is currently no accepted technology for inspecting the quality of the bondline, the application of bonded repairs to primary structure is limited [21,22]. Another issue with adhesive repairs is the lack of inspection method and analytical solution as well as damage tolerance information for ensuring the bondline integrity [6,23]. To credit a bonded patch repair of structural damage to primary aircraft structure, it must restore the static strength, stiffness, damage tolerance and fatigue performance of the original structure. Baker [20] characterised the bonded patch repair into two zones: the middle part of the repair was named ‘damage-tolerant zone’ and the tapered ends of the patch was called ‘safe-life zone’. Two types of joints, doubler overlap joint and skin doubler joint, were proposed as the generic joints to assess the damage tolerance of the damage-tolerant zone and the safe-life zone, respectively.

There have been studies on the damage tolerance of bonded composite patch repair under fatigue loading in the literature. However, most of the work was conducted on repairing of cracked aluminium adherends [19,20,24–26]. For example, the certification requirements on giving full credit to bonded carbon fibre patch repair in slowing crack growth and recovering residual strength of parent aluminium structure were addressed in [20]. Concerns were given to effects of fatigue and environmental durability on the patching efficiency. The skin doubler specimens were proposed

\* Corresponding author. Tel.: +61 3 9902 0113.

E-mail address: [wenyi.yan@monash.edu](mailto:wenyi.yan@monash.edu) (W. Yan).

in [20] for characterising the threshold for damage growth in the safe-life zone, which was used in the design of F111 repair in [27]. Charlkley et al. [24] presented an experimental study on the skin doubler specimens prepared by bonding composite skin doubler repair on aluminium adherend. The skin doubler consisted of eleven plies of unidirectional boron/epoxy and was bonded to the aluminium adherend by FM 73 adhesive. Since the purpose of the study was to determine the debonding initiation load, no initial flaw was introduced in the bondline. The specimens were subjected to constant amplitude fatigue load with a specific load ratio (min/max) at a frequency of 3 Hz. The disbond load was obtained when the strain at the doubler tip dropped by 10%. It reported that, the disbond initiation and propagation locations were dependent on the shape of the skin doubler tip. For skin doubler without a tapered tip (sharp end), the disbond was within the boron/epoxy ply adjacent to the adhesive bondline. For skin doubler repair with a tapered tip, the disbond tended to be mixed: some failure within the ply of boron/epoxy adjacent to the adhesive bondline and some failure at the interface between aluminium and adhesive. The disbond initiation loads of skin doubler repairs with different tip shapes indicated that adhesive stress was not a suitable parameter for describing the disbond initiation of the bondline. Poole [25] reported an experimental programme on the damage tolerance of skin doubler repairs to the cracked aluminium adherend under fatigue loading. Two types of skin doubler repairs were adopted: one was twelve plies unidirectional boron/epoxy patch and the other was sixteen plies unidirectional graphite/epoxy patch. The two patches were 132 mm long and 70 mm wide. Redux 312/5 was used as adhesive bonding the patches to the 2024-T3 aluminium panel of 145 mm wide and 4 mm thick. Initial flaw with a size of  $8 \times 10 \text{ mm}^2$  was embedded in the bondline at two locations. One was at the tip of the skin doubler repair and the other was located at the side edge of the skin doubler repair immediately covering the crack of the aluminium adherend. Specimens were tested under 110 MPa constant amplitude fatigue loading with a load ratio of 0.05. The experimental results indicated that no debond growth was detected for initial flaw at the tapered edge of the skin doubler repair until the aluminium panel fractured. When located at the side edge of the patch repair covering the crack of the aluminium panel, the initial flaw ( $8 \times 10 \text{ mm}^2$ ) grew with the aluminium crack under fatigue loading but had little effect on the fatigue life. Roach [26] reported a similar experimental program on the damage tolerance of boron/epoxy composite tapered skin doubler repair bonded to 2024-T3 aluminium adherend. The tapered skin doubler patch consisted thirteen plies boron/epoxy (type 5521/4) with a stacking sequence of  $(0/+45/-45/90)_3$ . FM-3 was used as adhesive. The stiffness ratio between skin doubler and aluminium was 1.2. The initial flaw (0.75" or 1" diameter) at the tip of the skin doubler repair was created by Teflon tape. Specimens were tested under fatigue loading at a range of 25.86–143.06 MPa. The experimental results showed that the large initial bondline flaw at the tip of the tapered skin doubler repair did not decrease the overall composite doubler performance. The size of the initial flaw remained almost unchanged until the fracture of the cadmium plate under fatigue loading.

It should be noted that, the above mentioned studies were all conducted on the damage tolerance of skin doubler repairs when bonded to aluminium adherends. Considering the increasing use of the fibre composite in airplane primary structures, it is necessary to understand the damage tolerance of skin doubler repairs when bonded to composite adherends. However, the existing experiences in aluminium adherends cannot be directly transferred to composite adherends which may have different debonding and damage mechanisms. This paper presents an experimental study on the damage tolerance of tapered skin doubler repairs

bonded on graphite/epoxy laminate adherend when subjected to fatigue loading.

Two types of tapered skin doubler joints, representative of repairs, were compared in this paper, named stepped doubler and ply-drop doubler, in terms of sensitivity of their fatigue behaviours to the embedded initial bondline flaw. Various initial flaws were introduced in the doubler bondline, by changing the flaw length and flaw width. Constant amplitude fatigue loading was determined through laminate coupon tests, to ensure a microstrain of 2800 is obtained in the laminate adherends under the peak load. The crack propagation was monitored and measured by a microscope during the fatigue loading. Fatigue life was determined when the crack reached a length of 100 mm. If there was no crack growth or the crack grew but did not reach the length of 100 mm, the fatigue loading was applied continuously up to 180,000 cycles. The failure modes, fatigue life and microscope observations of the crack initiation of both stepped and ply-drop doublers were reported and compared. The results of the work provide fatigue performance data that can be used to aid repair design, and to validate analysis methods.

## 2. Experimental program

### 2.1. Materials

Unidirectional graphite/epoxy ply of IM7/977-3 was used to prepare the laminate adherend and the skin doubler repair. The material properties adopted in subsequent analysis are based on those from Ref. [28] and listed in Table 1. Film adhesive FM300-2K was used to bond the doubler repair to the laminate adherend. The nominal weight of FM300-2K is 391 gsm with a nominal thickness of 0.33 mm. The lap shear strength at 24 °C is 40.7 MPa [29].

### 2.2. Skin doubler joint specimens with initial flaws

Thirty plies of IM7/977-3 were used to prepare the adherend and doubler laminate with a stacking sequence of  $[45/0/0/-45/90]_{35}$ . This layup represents laminate more likely found in an aircraft structure (eg. wing skin) where the layup has been optimised. Each ply of IM7/977-3 is 0.13 mm thick resulting in a nominal thickness of 3.9 mm for both laminate adherend and skin doubler repair.

Two types of doubler repair were selected. The first configuration (referred to as a “stepped taper” herein) is achieved by terminating each successive ply in the patch at a fixed distance short of the preceding ply. With this configuration, the first ply of the repair (adjacent to the bondline) is the longest ply. The second configuration (referred to as a “ply-drop taper” herein) is achieved with the shortest ply being placed adjacent to the bondline and each subsequent ply extending a fixed length beyond the preceding ply. The recommended doubler design is generally the ply-drop doubler, however there may be instances where the stepped doubler configuration is adopted, particularly if laminating/bonding pre-cured straps (e.g. battle damage repair [25]). The doubler panel was manufactured by staggering equal-size plies with a 3 mm offset to achieve the stepped taper at one end, and the ply-drop taper at the other, as shown in Fig. 1.

The parent laminate was manufactured in the same process as the skin doubler panel but without tapered ends. The top and bottom surfaces of the parent laminate were made smooth with a caul plate, whilst the top surface of the doubler panel was prepared with a silicon intensifier. When bonding the tapered skin doubler repair to the parent laminate, the adhering surfaces of the panels were degreased with Methyl Ethyl Ketone (MEK). Then FM300-2K was used as adhesive and cured under full vacuum condition in an oven at 125 °C for 120 min. The detailed configurations

**Table 1**  
Material data of IM7/977-3.

Properties	Unit	Value
Longitudinal modulus	MPa	164,100
Transverse modulus	MPa	9860
In-plane shear modulus	MPa	4950
Out-of-plane shear modulus	MPa	2944
Longitudinal Poisson's ratio	–	0.33
Transversal Poisson's ratio	–	0.34

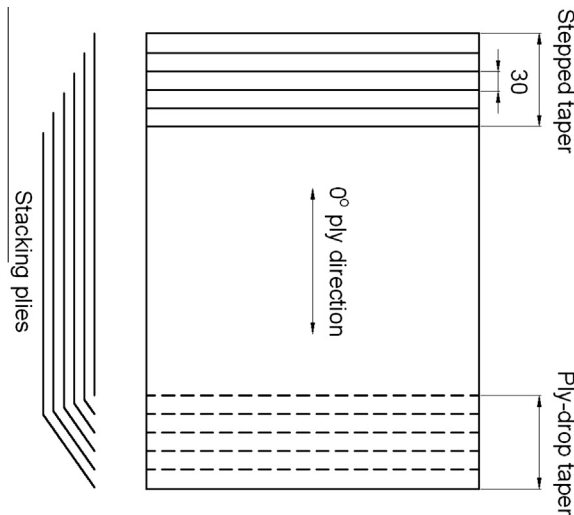


**Fig. 1.** Schematic of tapered panel manufacture.

of stepped and ply-drop doublers are shown in Fig. 2, with the doubler repair above the bondline (red line in Fig. 2) and parent laminate under the bondline.

The cured skin doubler repaired laminate panel was cut into strips of 360 mm long and 20 mm wide. The initial flaws at the tip of the tapered skin doubler repair were introduced using sheets of Teflon, secured with tape on the parent laminate during bonding of the doubler. Two types of initial flaws were prepared with one

through width flaw (20 mm wide the same as the width of the specimen), and the other partial width flaw (5 mm wide and 5 mm long). Three lengths were selected for the full width flaw, which were 5 mm, 10 mm and 20 mm. A “pristine” control specimen without an artificial flaw was also prepared for comparison purposes. The detailed dimensions of the skin doubler repaired specimen, as well as the location and dimensions of the full width flaw and partial width flaw are shown in Fig. 3. As can be seen in Fig. 3, a spacer (cut from the same panel as the parent laminate) of 70 mm long, 20 mm wide and 3.9 mm thick was bonded on the other end of the specimen. This was for clamping purpose when applying the fatigue loading, to avoid any loading eccentricity.

For each of the four initial flaw sizes, three identical specimens were prepared for repeating purpose. Three control specimens without initial flaw were also manufactured for comparison purpose. Therefore, a total of thirty specimens were prepared with fifteen stepped doubler repaired specimens and fifteen ply-drop doubler repaired specimens. The specimens with flaw length and flaw width are listed in Table 2. Each specimen has a label of ‘A-Length × Width-ID’, where the first letter represents the doubler type (i.e. ‘S’ for stepped doubler and ‘P’ for ply-drop doubler), followed by the flaw size (Length × Width), and the last number indicates the ID of repeating specimen.

### 2.3. Determination of fatigue loading

It was required that a strain of  $2800 \mu\epsilon$  should be achieved on the surface of the parent laminate adherend under the maximum fatigue loading. This strain level was chosen to match other fatigue tests performed within the project, and provided an accelerated but representative fatigue loading for a military aircraft, where one lifetime equals 30,000 cycles. Therefore, static coupon tests were conducted to determine the maximum amplitude of fatigue loading.

The laminate coupon was made of forty plies of IM7/977-3 with the same stacking sequence as the parent laminate of  $[45/0/0/-45/90]_{4S}$ . The coupon was 400 mm long. The measured width and thickness were 20.19 mm and 5.36 mm, respectively. The coupon tests were conducted on an Instron machine with a capacity of 50 kN. Two strain gauges were attached on both sides in the middle of the coupon. The strain gauges were CEA-06-

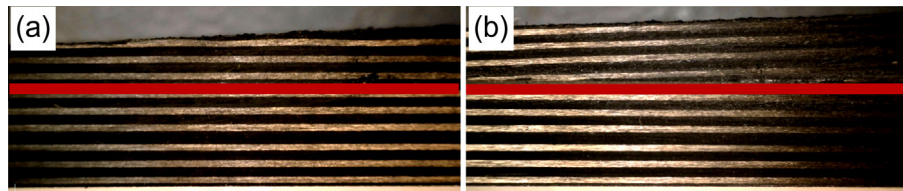


**Fig. 2.** (a) Stepped double; (b) ply-drop doubler (the red line represents the bondline). (For interpretation of the references to colour in this figure legend, the reader is referred to the web version of this article.)

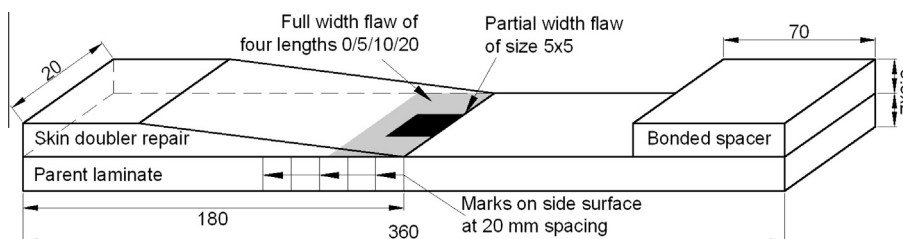


**Fig. 3.** Detailed dimensions of the skin doubler repaired specimen, and location and dimensions of the full width flaw and partial width flaw (unit in mm).

**Table 2**  
Specimens and main experimental results.

Specimen	Flaw width (mm)	Flaw length (mm)	Fatigue life (cycles)
S-Control-1	0	0	27,487
S-Control-2	0	0	24,798
S-Control-3	0	0	28,073
S-5 × 5-1	5	5	>180,000
S-5 × 5-2	5	5	>180,000
S-5 × 5-3	5	5	>180,000
S-5 × 20-1	5	20	>180,000
S-5 × 20-2	5	20	>180,000
S-5 × 20-3	5	20	>180,000
S-10 × 20-1	10	20	1143
S-10 × 20-2	10	20	1068
S-10 × 20-3	10	20	1516
S-20 × 20-1	20	20	391
S-20 × 20-2	20	20	320
S-20 × 20-3	20	20	200
P-Control-1	0	0	>180,000
P-Control-2	0	0	>180,000
P-Control-3	0	0	>180,000
P-5 × 5-1	5	5	>180,000
P-5 × 5-2	5	5	>180,000
P-5 × 5-3	5	5	>180,000
P-5 × 20-1	5	20	>180,000
P-5 × 20-2	5	20	>180,000
P-5 × 20-3	5	20	>180,000
P-10 × 20-1	10	20	2465
P-10 × 20-2	10	20	2380
P-10 × 20-3	10	20	2070
P-20 × 20-1	20	20	1044
P-20 × 20-2	20	20	783
P-20 × 20-3	20	20	1313

240UZ-120 from Vishay Microelectronics with a gage length of 6 mm and a gage factor of 2.09. The sensitive axes of the uniaxial gauges were parallel to loading direction for the measurement of tensile strains.

The test was in displacement control, at a speed of 0.5 mm/min. The coupon was tensioned from 0 kN up to 25 kN. Then the load was returned to 0 kN. The test was repeated for 10 times. The load and strain readings were recorded. The stress was calculated based on the measured coupon width and thickness. The readings of both strain gauges were averaged. Then the modulus of the coupon was determined based on the stress–strain relationship. The measured modulus of the laminate coupon was 85.6 GPa. Considering the requirement of 2800  $\mu\epsilon$  on the parent laminate, the maximum fatigue loading was determined as 18.7 kN.

#### 2.4. Experimental setup and instrumentations of fatigue tests

The fatigue tests on both stepped and ply-drop doubler repaired specimens were conducted on a fatigue machine of Instron 1342 with a loading capacity of 100 kN. Constant amplitude fatigue loading was applied from 1.87 kN to 18.7 kN with a load ratio of 0.1 (min/max) and a frequency of 3 Hz. The load, displacement and number of cycles were recorded by MTS FlexTest 40 Station Manager program, version 5.25A2912.

For the first several tests, one strain gauge was attached on the parent laminate of the specimen to ensure that the required 2800  $\mu\epsilon$  can be achieved under the maximum fatigue loading. The strain gauges are FLA-3-11-3LT from Tokyo Sokki Kenkyujo Co., Ltd. The gauge resistance is 119.5  $\Omega$ . The gauge factor is 2.1% and the gauge length is 3 mm. Before attaching the strain gauges, the bonding area on the laminate adherend was firstly polished using grit P240 Blue-Bak T417 waterproof sand paper from Norton Saint-Gobain. Then a finer sand paper with grit P400 was used to further polish the strain gauge bonding area. After cleaning the polished areas using Acetone, cyanoacrylate adhesive from Tokyo Sokki Kenkyujo Co., Ltd. was used to bond the strain gauges. The

gauge readings were transferred by DT85 data logger from Thermo Fisher Scientific Inc. The data was configured by DeTransfer 3.27 from dataTaker Pty Ltd. Then the gauge readings were recorded by DeFriend 2.6.1 program. The strain readings in Fig. 4 indicated that the required 2800  $\mu\epsilon$  was obtained at the maximum fatigue loading of 18.7 kN.

A microscope was used to monitor the crack propagation process and measure the crack length. The microscope was AD7013MZT from Dino-Lite Digital Microscope. It can capture detailed images with up to 2592 × 1944 pixels resolution. The magnification capacity was up to 250 times. The microscope was connected to a desktop through USB connection and the images can be captured and recorded by DinoCapture 2.0 program. In order to monitor the crack propagation during the fatigue loading using the microscope, one side of each skin doubler repaired specimen was painted in white using a correction pen. Six marks were made on the white painting with a spacing of 20 mm, with the first mark denoted the location of the doubler tip (see Fig. 3). The fatigue life of each specimen was defined as the number of cycles when the crack reached the final mark (100 mm from doubler tip). If there was no crack growth or the crack grew but did not reach the length of 100 mm, the fatigue loading was applied continuously up to six lifetimes (180,000 cycles). The experimental setup of the fatigue tests is shown in Fig. 5.

### 3. Experimental results and discussions

#### 3.1. Failure modes

Ply-drop doubler repaired specimens failed (the crack reaching 100 mm) when the flaw size was 10 × 20 mm<sup>2</sup> or 20 × 20 mm<sup>2</sup>. For specimens without initial flaw or when the flaw size was 5 × 5 mm<sup>2</sup> or 5 × 20 mm<sup>2</sup>, ply-drop doubler repaired specimens did not fail even after six lifetimes (180,000 cycles). Similarly, stepped doubler repaired specimens failed when the initial flaw size was 10 × 20 mm<sup>2</sup> or 20 × 20 mm<sup>2</sup>. An interesting observation was that the stepped specimens with an initial flaw size of 5 × 5 mm<sup>2</sup> or 5 × 20 mm<sup>2</sup> survived after 180,000 cycles, whilst specimens without initial flaw failed. The typical failure modes of specimens with a stepped doubler repair and ply-drop doubler repair are shown in Figs. 6 and 7, respectively. It also should be noted that, only part of the crack was shown up to the third mark, e.g. mark 1 denotes the doubler tip, mark 2 is 20 mm away from mark 1, and 3 is 40 mm away from mark 1.

For failed specimens, it can be seen in Figs. 6 and 7 that the crack started from the initial embedded flaw and propagated along

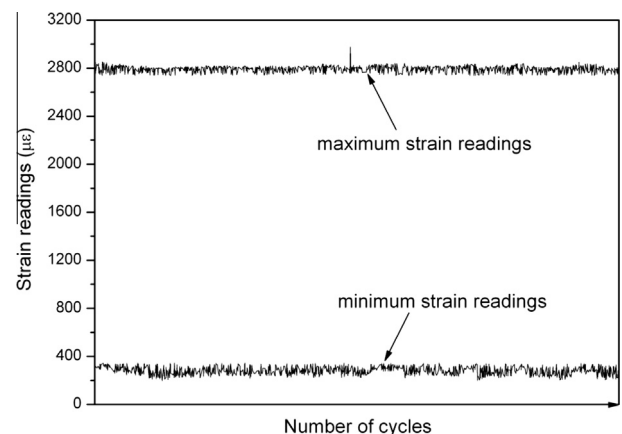


**Fig. 4.** Maximum and minimum strain readings against the number of cycles of specimen S-Control-2.

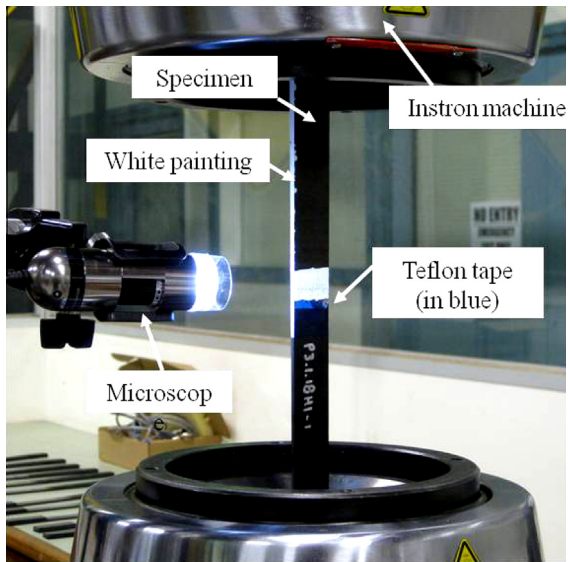


Fig. 5. Experimental set up of fatigue testing on the doubler repaired specimens.

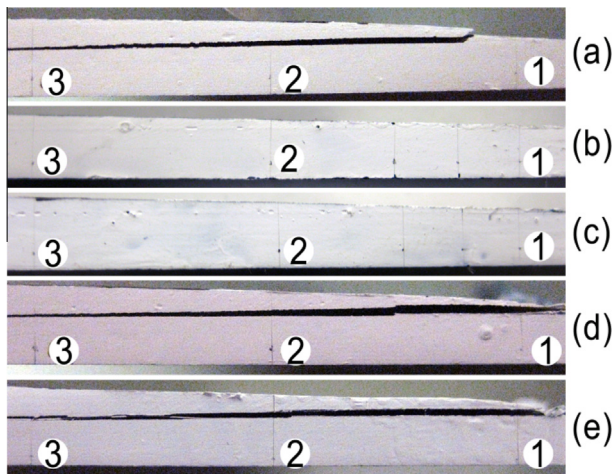


Fig. 6. Failure modes of specimens with stepped doubler repair with a flaw size of (a) without initial flaw; (b)  $5 \times 5 \text{ mm}^2$ ; (c)  $5 \times 20 \text{ mm}^2$ ; (d)  $10 \times 20 \text{ mm}^2$ ; (e)  $20 \times 20 \text{ mm}^2$ .

the adhesive bondline for both stepped and ply-drop doubler repaired specimens. One observation which needs special attention is for stepped doubler specimen without an initial flaw. The specimen failed with the crack initiated some distance away from the doubler tip (Fig. 6a). For specimens that did not fail (i.e. exceeding 180,000 cycles) no crack growth was visible (see Figs. 6b, c and 7a–c). Detailed microscope investigations on the crack initiation and propagation patterns will be presented in Section 3.3.

### 3.2. Crack propagation and fatigue life

The crack propagation process of the failed specimens was recorded and measured by the microscope. The measured crack propagation length against the corresponding number of cycles was plotted in Fig. 8. The left side of Fig. 8 shows the crack propagation curves of failed specimens with an initial flaw ( $10 \times 20 \text{ mm}^2$  or  $20 \times 20 \text{ mm}^2$  size), and the right side presents the crack propagation curves of specimens (stepped doubler) without an initial flaw. It should be noted that, the crack length in Fig. 8 was



Fig. 7. Failure modes of specimens with ply-drop doubler repair with a flaw size of (a) without initial flaw; (b)  $5 \times 5 \text{ mm}^2$ ; (c)  $5 \times 20 \text{ mm}^2$ ; (d)  $10 \times 20 \text{ mm}^2$ ; (e)  $20 \times 20 \text{ mm}^2$ .

measured from the tip of doubler repair including the length of the initial flaw.

For failed specimens with an initial flaw, a three-stage crack propagation process was identified from the left side of Fig. 8. In the first stage, the crack grew slowly before it reached a length of about 30 mm. In the second stage, the crack growth became unstable after it exceeded 30 mm and it grew rapidly until 90 mm. Finally, the crack growth rate reduced again until the final 100 mm length was reached. For stepped doubler repaired specimens without an initial flaw (right side of Fig. 8), a two-stage crack propagation process was observed, with the crack firstly grew slowly until 30 mm after which the crack growth became unstable. The reduction of crack growth rate (as shown in the third stage of specimens with an initial flaw) was not observed for specimens without an initial flaw. It seems that for both stepped and ply-drop doubler repaired specimens in the current study, 30 mm is a critical crack length beyond which catastrophic bondline failure becomes inevitable. In addition, stepped doubler repaired specimens with an initial flaw of 20 mm long (S- $20 \times 20$ ) failed rapidly as soon as the fatigue load was applied, without experiencing the first stage of slow crack growth.

The fatigue life of each failed specimen was defined as the number of cycles when the crack reached 100 mm length (measured from the tip of the doubler repair). The fatigue life of each specimen is listed in Table 2. When the specimen survived six lifetimes, its fatigue life is denoted as '>180,000' cycles in Table 2. The fatigue lives of three identical specimens are averaged and plotted against the size of initial flaw for stepped and ply-drop doubler repaired specimens in Fig. 9.

As can be seen from Table 2 and Fig. 9, there is a general trend that the fatigue life decreases with the increase of initial flaw size for both stepped and ply-drop doubler repaired specimens. It is also obvious from Table 2 and Fig. 9 that, ply-drop doubler repair performed better than stepped doubler repair in terms of damage tolerance under fatigue loading. For example, the ply-drop doubler repair without an initial flaw (P-Control) survived after six lifetimes (>180,000 cycles), comparing to the stepped doubler counterpart (S-Control) which failed at an average fatigue life of 26,786 cycles. Both stepped and ply-drop doubler repaired specimens survived six lifetimes (>180,000 cycles) when the imbedded flaw length was 5 mm. At an initial flaw size of  $10 \times 20 \text{ mm}^2$ , the ply-drop doubler repair (P- $10 \times 20$ ) achieved an average fatigue life of 2,305 cycles, which is almost twice the average fatigue life (1,242 cycles) of the stepped doubler repair (S- $10 \times 20$ ). When

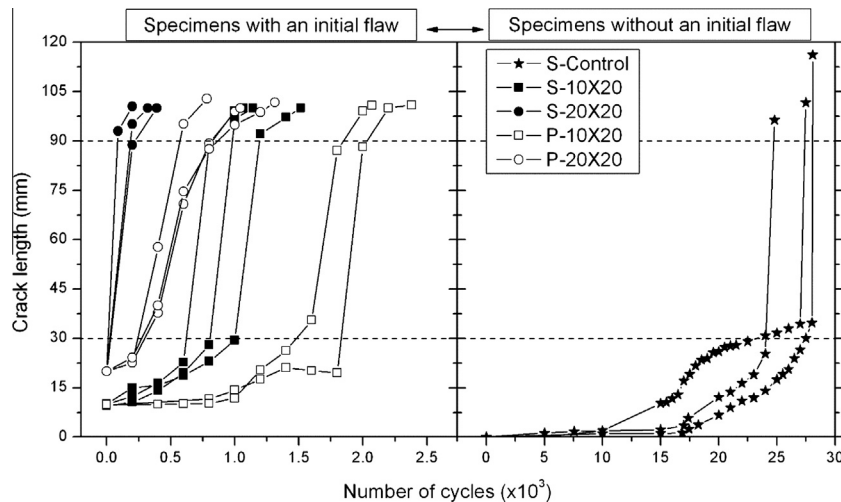


Fig. 8. Crack propagation of failed stepped doubler (solid symbols) and ply-drop doubler (hollow symbols) repaired specimens.

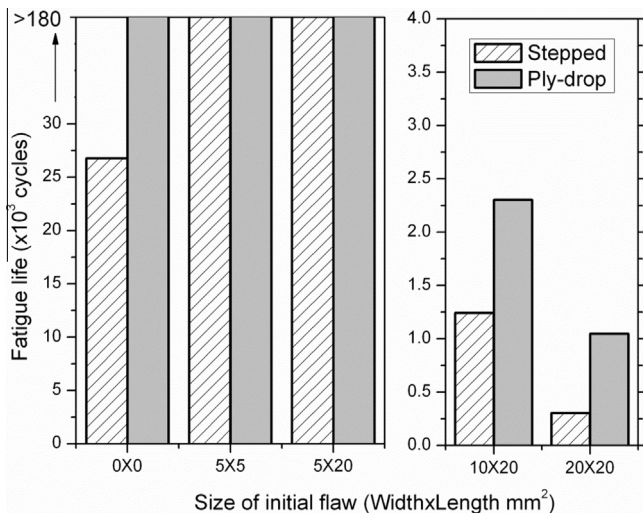


Fig. 9. Average fatigue life versus size of initial flaw for stepped and ply-drop doubler repaired specimens.

the embedded flaw size increased to  $20 \times 20 \text{ mm}^2$ , the fatigue life of the P- $20 \times 20$  (1,047 cycles) dropped by 55% comparing to that of P- $10 \times 20$ . On the other hand, the S- $20 \times 20$  could only sustain an average fatigue life of 304 cycles (around one third that of P- $20 \times 20$ ), showing a drop by 77% comparing to S- $10 \times 20$ .

One unexpected observation is that the stepped doubler repair without an initial flaw (S-Control) surprisingly failed at 26,786 cycles, whilst it survived six lifetimes ( $>180,000$  cycles) with an initial flaw of 5 mm long (5 mm wide or 20 mm wide). The authors hypothesize that specimens without an initial flaw had the crack initiated from a point on the tapered doubler which was some distance away from the doubler tip, such as the termination of the first  $0^\circ$  ply. The introduction of an embedded flaw of 5 mm length suppressed the crack initiation tendency on the tapered doubler and shifted the crack initiation to the tip of the initial flaw. As mentioned in Section 3.1, evidences on the different crack initiation location of stepped doubler specimens without an initial flaw were observed from visual inspection (see Fig. 6a). However, more detailed microscope investigations on the crack initiation and propagation pattern are necessary to support the hypothesis.

### 3.3. Microscope investigation of the crack initiation and propagation

Microscope AD7013MZT from Dino-Lite Digital Microscope was used to investigate the detailed crack initiation and propagation patterns of failed specimens. The magnification of the microscope was 50 times at a resolution of  $1280 \times 960$  pixels. The crack initiation and propagation patterns for failed ply-drop doubler repaired specimens are presented in Fig. 10, where the initial flaw (Teflon tape) is highlighted by a blue<sup>1</sup> line and the crack is indicated by green lines. As can be seen in Fig. 10, the crack initiated from the tip of the Teflon film, then grew at the interface between the adhesive and the  $45^\circ$  ply of the parent laminate. After a short while, the crack passed the  $45^\circ$  ply and propagated at the interface between  $45^\circ$  and  $0^\circ$  plies in the adherend laminate.

The crack initiation and propagation patterns of failed stepped doubler repaired specimens with an initial flaw of  $10 \times 20 \text{ mm}^2$  or  $20 \times 20 \text{ mm}^2$  are shown in Fig. 11. Similar to failed ply-drop doubler repaired specimens with the same size of initial flaw, the crack also started from the tip of Teflon tape and grew at the interface between the adhesive and the  $45^\circ$  ply of the parent laminate. The crack passed the  $45^\circ$  ply shortly and propagated at the interface between  $45^\circ$  ply and  $0^\circ$  ply of the adherend laminate till failure.

A different crack initiation and propagation pattern of failed stepped doubler repaired specimen without an initial flaw is identified in Fig. 12(a) and (b). When there is no initial flaw, the crack initiated from the tip of the first  $0^\circ$  ply in the doubler (Fig. 12a) adjacent to the adhesive bondline. The crack then grew at the interface between the  $0^\circ$  ply and the  $45^\circ$  ply in the doubler for a while, before it passed the  $45^\circ$  ply in the doubler and entered the adhesive bondline (Fig. 12b). After passing the adhesive bondline, the crack grew a short distance at the interface between the adhesive and  $45^\circ$  ply in the adherend laminate (Fig. 12b). Finally the crack steadily propagated at the interface between the  $0^\circ$  ply and  $45^\circ$  ply in the adherend laminate.

For comparison purpose, the microscope image of stepped doubler repaired specimen with an initial flaw of  $5 \times 20 \text{ mm}^2$  is presented in Fig. 12(c). As can be seen, no crack initiation or propagation was observed in the doubler repair adjacent to the adhesive bondline. The crack initiated at the tip of initial flaw and only grew a very limited distance after 180,000 cycles of fatigue loading.

<sup>1</sup> For interpretation of color in Fig. 10, the reader is referred to the web version of this article.

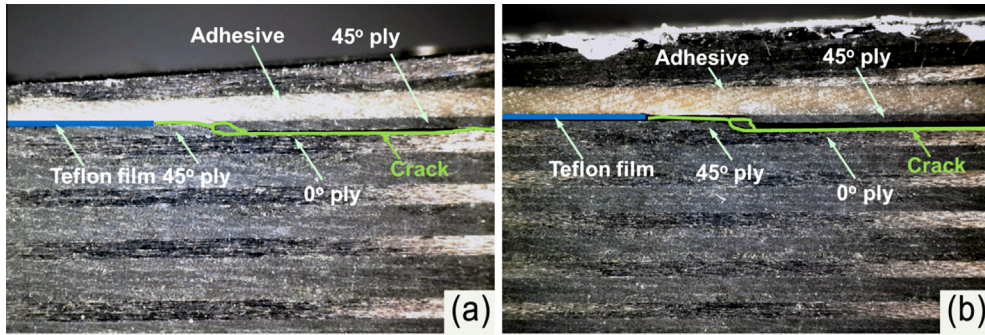


Fig. 10. Crack initiation and propagation pattern of failed ply-drop doubler repaired specimens with an initial flaw of (a)  $10 \times 20 \text{ mm}^2$  and (b)  $20 \times 20 \text{ mm}^2$ .

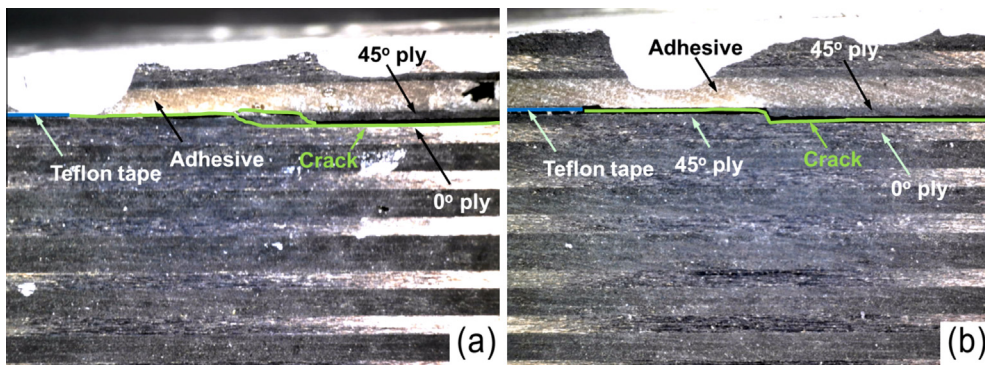


Fig. 11. Crack initiation and propagation pattern of failed stepped doubler repaired specimens with an initial flaw of (a)  $10 \times 20 \text{ mm}^2$  and (b)  $20 \times 20 \text{ mm}^2$ .

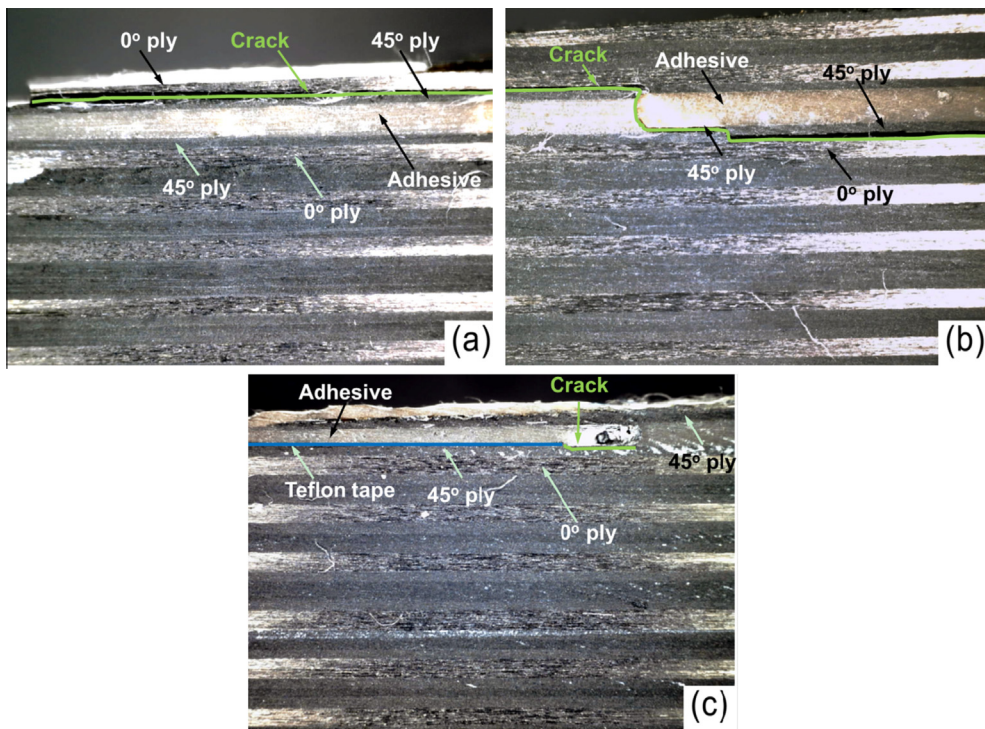


Fig. 12. (a) Crack initiation and propagation pattern of stepped doubler repaired specimens, (b) without an initial flaw and (c) with an initial flaw of  $5 \times 20 \text{ mm}^2$ .

According to the microscope observations shown in Figs. 10–12, several conclusions can be drawn: firstly, when there was an initial bondline flaw of the size  $10 \times 20 \text{ mm}^2$  or  $20 \times 20 \text{ mm}^2$ , both stepped and ply-drop doubler repaired specimens experience the

same crack initiation and propagation pattern. The crack always initiated from the tip of the bondline flaw and propagated for a short distance at the interface between adhesive and  $45^\circ$  ply in the parent adherent. The crack finally grew at the interface

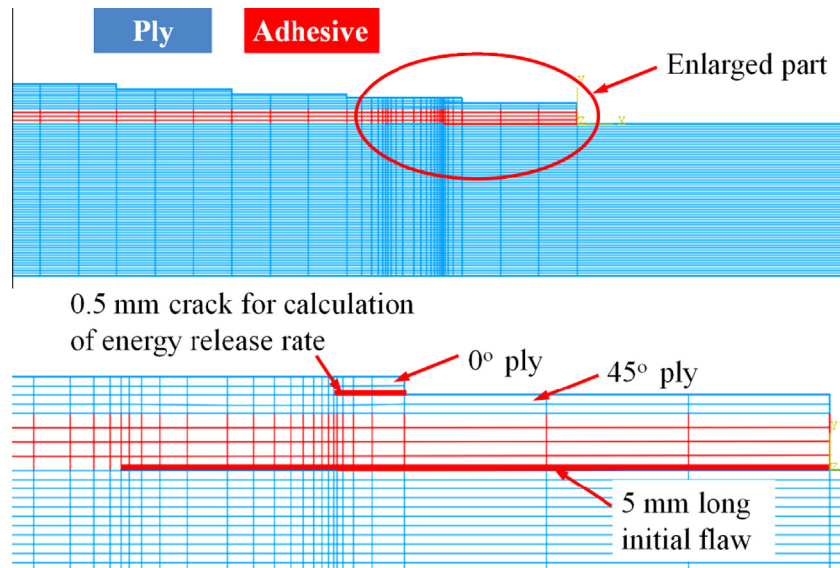


Fig. 13. Mesh details and crack geometries (model with 5 mm initial flaw).

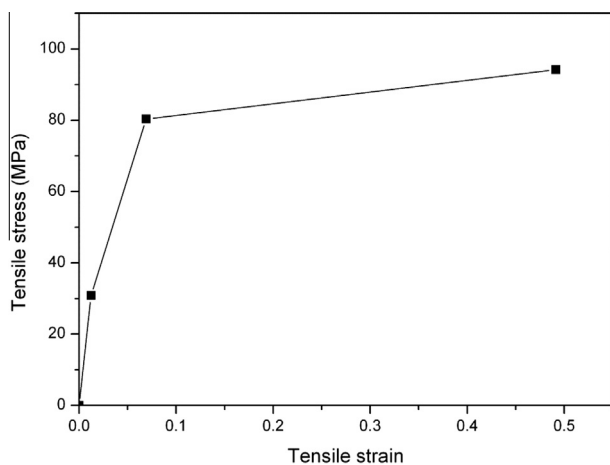


Fig. 14. Stress–strain relationship of adhesive FM300-2K in FE models.

between 45° ply and 0° ply in the adherend laminate until complete failure of the specimen. Secondly, when there was no embedded bondline flaw, stepped doubler repaired specimen also failed due to the crack initiation at the tip of the first 0° ply in the doubler adjacent to the adhesive bondline. After a short distance propagation at the interface between 0° ply and 45° ply in the doubler, the crack passed the adhesive bondline and finally entered and grew at the interface between 45° ply and 0° ply in the adherend laminate. Thirdly, when an initial bondline flaw with a length of 5 mm was introduced in the stepped doubler repair, the tendency of crack initiation in the doubler was suppressed. Instead, the crack initiated at the flaw tip and only grew for a limited length under the fatigue loading up to 180,000 cycles. It seems that the introduction of an initial bondline flaw of 5 mm length suppressed the crack initiation tendency in the doubler.

#### 3.4. Finite element simulations of the stepped doubler repair

Finite element simulations were conducted using Abaqus. The purpose is to provide numerical evidence of the observations for stepped doubler in Section 3.3. Two FE models were built: one was stepped doubler without an initial flaw and the other one

was stepped doubler with a 5 mm initial flaw. In both models, 8-node linear brick elements, C3D8R, with reduced integration were used for both ply and adhesive materials. Two elements were used for each ply and four elements for the adhesive bondline (see Fig. 13) which was determined through mesh sensitivity study. The material properties of a ply as listed in Table 1 were adopted in both FE models. For the adhesive FM300-2K, its stress strain relationship under room temperature as shown in Fig. 14 was used [29].

The two models had the same geometry as shown in Fig. 3. The left end of the specimen was fixed in all directions and the right end was also fixed in all directions except the movement in longitudinal direction of the specimen. A load of 18.7 kN was applied at the right end of the specimen simulating the maximum fatigue loading in the experiments (for the reference of the left and right ends, please see Fig. 3). The energy release rate ( $G$ ) at the tip of the first 0° ply of the doubler was calculated based on the contour integral method in Abaqus, assuming a small initial crack of 0.5 mm at the location of interest (see Fig. 13). In the following discussions,  $G_0$  means the energy release rate of the stepped doubler without initial bondline flaw and  $G_5$  is the energy release rate of the stepped doubler with a 5 mm initial bondline flaw. The FE results showed that the specimen without an initial bondline flaw had an energy release rate ( $G_0$ ) of 230 J/m<sup>2</sup> at the tip of the first 0° ply. In contrast, the 5 mm initial bondline flaw effectively unloaded this critical location in the patch, resulting in an energy release rate ( $G_5$ ) value of only 1.42 J/m<sup>2</sup>.

The calculated energy release rate at the tip of the first 0° ply in the pristine specimen of 230 J/m<sup>2</sup> exceeds the threshold strain energy release rate for mode II fatigue crack growth measured for the same material of 180 J/m<sup>2</sup> [30], which is consistent with the experimental results presented herein showing crack growth from this location for the step doubler specimens without initial bondline flaws.

#### 4. Conclusions

An experimental program on the damage tolerance behaviour of tapered skin doubler repair of graphite/epoxy laminate under fatigue loading was presented. Two types of skin doubler repairs were selected and compared, namely stepped doubler repair and ply-drop doubler repair. Various initial flaws were embedded in

the bondline at the tip of doubler repair by changing the flaw length and width. Constant amplitude fatigue loading was applied to all doubler repaired specimens. The fatigue life of specimen was recorded and the crack growth against the number of cycles was presented. The crack initiation and propagation patterns of failed specimens were studied through microscope investigations. Based on the current experimental results, the following conclusions can be drawn:

- Ply-drop doubler joints consistently performed better than stepped doubler joints in terms of damage tolerance under fatigue loading. When there was no initial bondline flaw, the ply-drop doubler specimen survived 180,000 cycles fatigue loading, while the stepped doubler counterpart failed at an average fatigue life of 26,786 cycles. With an initial bondline flaw, the ply-drop doubler specimens lasted approximately 2–3 times longer than the equivalent stepped doubler specimens.
- For both taper designs, slow crack growth was observed until the crack reached approximately 30 mm in length, after which crack growth was very rapid.
- The investigation on the crack initiation and propagation patterns for failed specimens showed that, when there was an embedded bondline flaw, the crack always initiated from the flaw tip. The microscope studies also indicated that the interface between 45° ply and 0° ply in the adherend laminate was a fatigue critical plane, because the crack always ended up propagating at this interface until failure. This is expected given that the interlaminar fracture toughness of composite laminates can be an order of magnitude lower than that of a structural film adhesive [31].
- The stepped doubler is not a desirable configuration for skin doubler repair applications, because it failed within one life time even without an initial bondline flaw. Microscope observations showed that the failure was attributed to the crack initiation and propagation at the interface between 45° ply and 0° ply in the tapered doubler tip adjacent to the adhesive bondline. FE simulations agreed well with the experimental observations, supporting observations that a crack would grow under fatigue loading in the doubler with a pristine bondline, and that the introduction of a bondline flaw would relieve this critical location.
- A damage tolerant repair design must be able to withstand the fatigue requirements of the repaired structure, assuming the presence of damage at the threshold of detection. The experimental results in this paper suggest that when considering doubler tip flaws, an inspection technology should be adopted capable of detecting damage down to a threshold size of 5 mm. This is achievable with conventional ultrasonic inspection methods [32].

## Acknowledgments

This work was undertaken within the Robust Composite Repairs project, part of a CRC-ACS research program, established and supported under the Australian Government's Cooperative Research Centres Program. The authors acknowledge the assistance of Mr. Mick Crossthwaite (ACS Australia) for the manufacture of all test specimens, using the facilities of ACS Australia and Defence Science and Technology Organisation (DSTO). Lab manager Mr. Alan Coram at the Department of Mechanical and Aerospace Engineering in Monash University is also acknowledged for his assistance in organising the fatigue testing facilities.

## References

- [1] Kimiaieifar A, Lund E, Thomsen OT, Sørensen JD. Asymptotic sampling for reliability analysis of adhesive bonded stepped lap composite joints. *Eng Struct* 2013;49:655–63.
- [2] Keller T. Use of fiber reinforced polymers in bridge construction. *Structural engineering documents* 7. In: International association for bridge and structural engineering (IABSE), Zurich, Switzerland; 2003.
- [3] Hollaway L. *Polymer composites for civil and structural engineering*. London: Chapman & Hall; 1993.
- [4] Wu C, Bai Y. Web crippling behaviour of pultruded glass fibre reinforced polymer sections. *Compos Struct* 2014;108:789–800.
- [5] Satasivam S, Bai Y, Zhao XL. Adhesively bonded modular GFRP web-flange sandwich for building floor construction. *Compos Struct* 2014;111:381–92.
- [6] Odi RA, Friend CM. A comparative study of finite element models for the bonded repair of composite structures. *J Reinf Plast Compos* 2002;21(4):311–32.
- [7] Liu X, Wang G. Progressive failure analysis of bonded composite repairs. *Compos Struct* 2007;81(3):331–40.
- [8] Cheng PC, Gong XJ, Hearn D, Aivazzadeh S. Tensile behaviour of patch-repaired CFRP laminates. *Compos Struct* 2011;93(2):582–9.
- [9] Atas C, Akgun Y, Dagdelen O, Icten BM, Sarikanat M. An experimental investigation on the low velocity impact response of composite plates repaired by VARIM and hand lay-up processes. *Compos Struct* 2011;93(3):1178–86.
- [10] Caminero MA, Pavlopoulou S, Lopez-Pedrosa M, Nicolaisson BG, Pinna C, Soutis C. Analysis of adhesively bonded repairs in composites: damage detection and prognosis. *Compos Struct* 2013;95:500–17.
- [11] Kim JH, Park BJ, Han YW. Evaluation of fatigue characteristics for adhesively-bonded composite stepped lap joint. *Compos Struct* 2004;66(14):69–75.
- [12] Beylergil B, Aktas A, Cunedioglu Y. Buckling and compressive failure of stepped-lap joints repaired with composite patches. *J Compos Mater* 2012;46(26):3213–30.
- [13] Wahab MMA. Fatigue in adhesively bonded joints: a review. *ISRN Mater Sci* 2012. <http://dx.doi.org/10.5402/2012/746308>.
- [14] Katnam KB, Silva LFMD, Young TM. Bonded repair of composite aircraft structures: a review of scientific challenges and opportunities. *Prog Aerosp Sci* 2013;61:26–42.
- [15] Kim HS, Lee SJ, Lee DG. Development of a strength model for the cured stepped lap joints under tensile loading. *Compos Struct* 1995;32:593–600.
- [16] Wu C, Zhao XL, Duan WH, Al-Mahaidi R. Bond characteristics between ultra high modulus CFRP laminates and steel. *Thin-Walled Struct* 2012;51:147–57.
- [17] Banea MD, Silva LFMD. Adhesively bonded joints in composite materials: an overview. *Proc Inst Mech Eng Part L – J Mater-Des Appl* 2009;223(L1):1–18.
- [18] Hale J. Boeing 787 from the ground up. *Aero Mag Boeing* 2006;24(4):17–23.
- [19] Alderliesten RC. Damage tolerance of bonded aircraft structures. *Int J Fatigue* 2009;31(6):1024–30.
- [20] Baker A. Bonded composite repair of fatigue-cracked primary aircraft structure. *Compos Struct* 1999;47(1–4):431–43.
- [21] Baker A, Gunnion AJ, Wang J. On the certification of bonded repairs to primary composite aircraft components. *J Adhes* 2014;91(1–2):4–38.
- [22] Bonded Repair Size Limits. FAA, PS-AIR-100-14-130-001, 24 November 2014.
- [23] Goh JY, Georgiadis S, Orifici AC, Wang CH. Effects of bondline flaws on the damage tolerance of composite scarf joints. *Compos A Appl Sci Manuf* 2013;55:110–9.
- [24] Chalkley PD, Wang CH, Baker AA. Fatigue testing of generic bonded joints. In: Baker AA, Rose LRF, Jones R, editors. *Advances in the bonded composite repair of metallic aircraft structure*. Oxford: Elsevier Science Ltd.; 2002. p. 103–26 [chapter 5].
- [25] Poole P. Graphite/epoxy patching efficiency studies. In: Baker AA, Rose LRF, Jones R, editors. *Advances in the bonded composite repair of metallic aircraft structure*. Oxford: Elsevier Science Ltd.; 2002. p. 415–41 [chapter 15].
- [26] Roach D. Damage tolerance assessment of bonded composite doubler repairs for commercial aircraft applications. In: Baker AA, Rose LRF, Jones R, editors. *Advances in the bonded composite repair of metallic aircraft structure*. Oxford: Elsevier Science Ltd.; 2002. p. 485–516 [chapter 17].
- [27] Baker AA, Rose LRF, Walker KF, Wilson ES. Repair substantiation for a bonded composite repair to F111 lower wing skin. *Appl Compos Mater* 1999;6(4):251–67.
- [28] Breitzman TD. Multiscale strain analyses. PhD thesis, Louisiana State University, USA, May 2005.
- [29] FM300-2 Technical Datasheet. Cytec Engineering Materials, April 2007.
- [30] Donough M. Load ratio effects in the fatigue crack propagation of composite laminates and bonded joints. PhD thesis, RMIT University, Australia, November 2014.
- [31] Baker AA. Repair technology. In: Baker AA, Dutton S, Kelly D, editors. *Composite materials for aircraft structures*. Reston, Virginia: American Institute of Aeronautics and Astronautics, Inc.; 2004. p. 369–402.
- [32] Chern EJ, Chu HP, Yang JN. Assessment of probability of detection of delaminations in fibre-reinforced composites. NASA Technical Memorandum 104553, December 1991.